Eur. Phys. J. A (2018) **54**: 67
DOI 10.1140/epja/i2018-12501-y

The European Physical Journal A

Regular Article – Experimental Physics

Activation cross section and isomeric cross section ratio for the ^{76}Ge(n, 2n)^{75m,g}Ge process

Junhua Luo[1,2,a], Li Jiang[3], and Xinxing Wang[2]

[1] Institute of New Energy, Hexi University, Zhangye 734000, China
[2] School of Physics and Electromechanical Engineering, Hexi University, Zhangye 734000, China
[3] Institute of Nuclear Physics and Chemistry, Chinese Academy of Engineering Physics, Mianyang 621900, China

Received: 3 December 2017 / Revised: 15 March 2018
Published online: 26 April 2018

Communicated by T. Motobayashi

Abstract. We measured neutron-induced reaction cross sections for the ^{76}Ge(n, 2n)^{75m,g}Ge reactions and their isomeric cross section ratios σ_m/σ_g at three neutron energies between 13 and 15 MeV by an activation and off-line γ-ray spectrometric technique using the K-400 Neutron Generator at the Chinese Academy of Engineering Physics (CAEP). Ge samples and Nb monitor foils were activated together to determine the reaction cross section and the incident neutron flux. The monoenergetic neutron beams were formed via the ^{3}H$(d,n)^4$He reaction. The pure cross section of the ground state was derived from the absolute cross section of the metastable state and the residual nuclear decay analysis. The cross sections were also calculated using the nuclear model code TALYS-1.8 with different level density options at neutron energies varying from the reaction threshold to 20 MeV. Results are discussed and compared with the corresponding literature data.

1 Introduction

Activation cross sections of neutron threshold reactions on medium mass nuclei are of considerable interest for testing nuclear models. Furthermore, the data for potential first wall constituents of a fusion reactor are of practical importance, especially for estimating nuclear heating, nuclear transmutation, and radiation damage effects [1]. A lot of experimental data on neutron induced cross sections for fusion reactor technology applications have been reported and great efforts have been devoted to compilations and evaluations [2,3]. We chose to study the neutron-induced reaction cross sections of germanium-76 mainly for four reasons. First, the germanium is an important semi-conducting material for the nuclear technology and integrated circuits; second, the ^{76}Ge nucleus lies between the magic numbers of 28 and 50; shape coexistence plays a prominent role in its structure [4], and ^{76}Ge may be a rare example of a nucleus exhibiting rigid triaxial deformation in its low-lying states [5,6]; third, the germanium-75 isomeric pair is an example of the isomeric pair type in which the half-life of the metastable state is shorter than that of the ground state and decays almost entirely by isomeric transition (see fig. 1); fourth, although there are enough data for metastable cross sections for the ^{76}Ge(n, 2n)^{75m}Ge reactions in the energy range from 13 to 15 MeV [7–14], only three direct measurements for the ground state cross section σ_g have been performed separately [7,9,14]. The experimental and theoretical data for the ^{76}Ge(n, 2n)^{75g}Ge reaction cross section are inconsistent. In the energy region around 14 MeV, the experimental cross sections [7,9,14] are clustered around 550 mb, while the results of TALYS are centered around 300 mb.

Therefore, we aimed to measure the pure ground state cross section σ_g directly by means of the analysis methods of residual nuclear decay [15–17] and to compare the experimental results to those obtained by the statistical model calculation.

[a] e-mail: luojh71@163.com

2 Experimental

2.1 Samples and irradiations

Two disks, about 0.1 and 0.19 cm in thickness and 20 mm in diameter, were formed by pressing approximately 1.7 and 3.2 g of Ge (99.99% pure) powder (natural isotopic composition) at 980 MPa to form a pellet. The samples were irradiated near the target and sandwiched between two Nb foils (99.99% pure, 0.12 mm thick) with the same diameter which were used to monitor the neutron fluence via the ^{93}Nb(n, 2n)^{92m}Nb reaction.

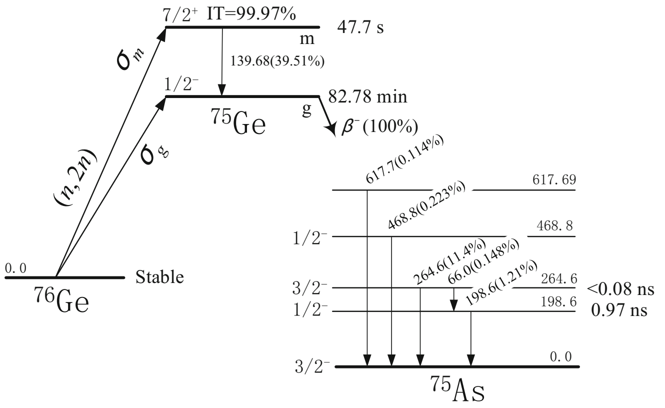

Fig. 1. Metastable and ground state formation in the reaction ^{76}Ge(n, 2n)$^{75\text{m,g}}$Ge [18]. All energies are in keV.

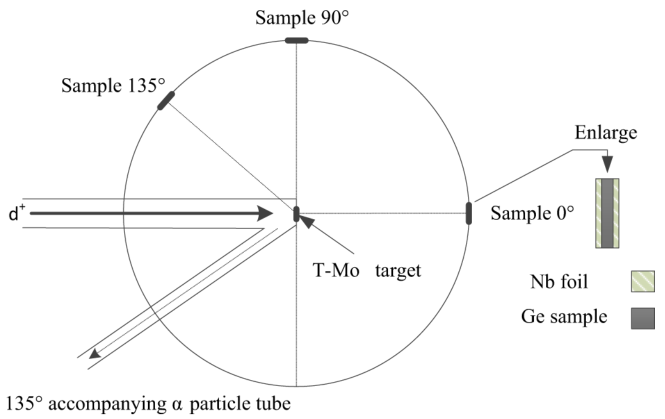

Fig. 2. Sketch of the experimental geometry. The Au-Si surface barrier detector used in α-particle tube was positioned at 135° and 110 cm from the target.

Irradiation of the samples was carried out at the K-400 Neutron Generator at the Chinese Academy of Engineering Physics (CAEP) and lasted approximately 3 minutes with a neutron yield (3–4)$\times 10^{10}$ n/s in 4π solid angle. Neutrons were produced by the T(d,n)^{4}He reaction with an effective deuteron beam energy of 135 keV, beam current of 240 μA, and the diameter of the deuteron beam spot was under 0.6 cm. The groups of samples were placed at 0°, 90° and 135° relative to the beam direction and centered a 0.566 mg/cm^2 thick tritium-molybdenum (T-Mo) target at a distance of $\sim$ 50 mm. In order to avoid the deposition of deuterium in the target, the new T-Mo target is used. The diameter of the active zone of the T-Mo target is 1.2 cm. The sample positions in the experiment are shown in fig. 2. In order to avoid the effect of low energy neutrons, samples were wrapped in cadmium foil. During irradiation, the neutron flux was monitored by accompanying α-particles so that corrections could be made for small variations of the yield. Cross sections for the ^{93}Nb(n, 2n)$^{92\text{m}}$Nb monitor reaction were taken from [19].

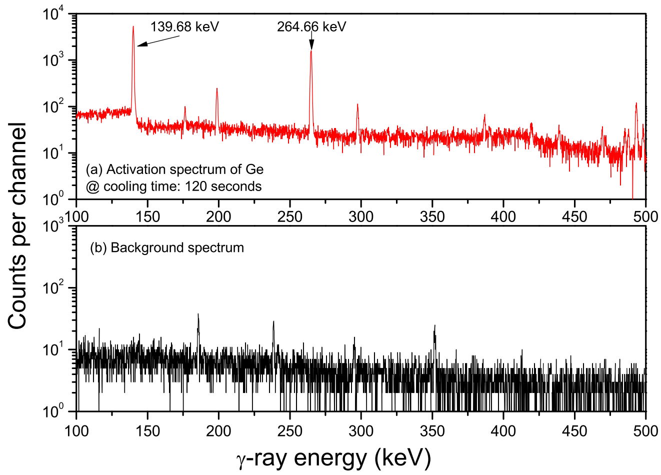

Fig. 3. (a) The γ-ray spectrum of germanium about 2 minutes after the end of irradiation; (b) the background spectrum.

2.2 Measurement of radioactivity

High-resolution gamma-ray spectroscopy was applied to the activated disks. The measurements were carried out using low-background high-purity germanium (HPGe) detector (ORTEC, model GEM 60P, crystal diameter 70.1 mm, crystal length 72.3 mm) with a relative efficiency of $\sim$ 68% and an energy resolution of 1.69 keV at 1.332 MeV for ^{60}Co. The distance from sample to detector was 2.0 cm. To avoid excessive death time, the sample was cooled for 2 minutes after irradiation. Figure 3 shows the typical spectra acquired from the Ge samples during the measurement of the isomeric and ground state, where the γ-rays of interest have been marked. The γ-ray intensities and half-lives used in the analysis are summarized in table 1 [18]. The detector was pre-calibrated for energy and efficiency by using the standard gamma ray sources ^{54}Mn, ^{57}Co, ^{60}Co, ^{109}Cd, ^{133}Ba, ^{137}Cs, ^{152}Eu, ^{241}Am and ^{226}Ra.

2.3 Calculation of cross sections and their uncertainties

The cross sections were calculated by the following formula [16,17]:

$$\sigma_x = \frac{[S\varepsilon I_\gamma \eta KMD]_0}{[S\varepsilon I_\gamma \eta KMD]_x} \cdot \frac{[\lambda AFC]_x}{[\lambda AFC]_0}\sigma_0, \qquad (1)$$

where the subscript 0 represents the term corresponding to the monitor reaction and subscript x corresponds to the measured reaction; ε is the full-energy peak efficiency of the measured characteristic gamma-ray; $I\gamma$ is the gamma-ray intensity; η is the abundance of the target nuclide; M is the mass of the sample; $D = e^{-\lambda t_1} - e^{-\lambda(t_1+t_2)}$ is the counting collection factor; $S = 1 - e^{-\lambda T}$ is the growth factor of the product nuclide, T is the total irradiation time; t_1 is the total cool time and t_2 is the total measurement time; A is the atomic weight; C is the measured full energy peak area; λ is the decay constant; K is the neutron

Table 1. Neutron induced nuclear reactions on germanium and niobium and decay data of associated activation products (taken from [18]).

Reaction	Abundance of target isotope (%)	Half-life of product	E-threshold (MeV)	Mode of decay (%)	E_γ (keV)	I_γ (%)
^{76}Ge(n, 2n)^{75m}Ge	7.73_{12}	47.7_5 s	9.694	IT(99.97)	139.68	39.51
^{76}Ge(n, 2n)^{75g}Ge	7.73_{12}	82.78_4 m	9.552	β(100)	264.6	11.4
^{93}Nb(n, 2n)^{92m}Nb	100	10.15_2 d	8.972	EC(100)	934.44	99.15

Table 2. Correction factors for the self-absorption of the sample at a given gamma-ray energy.

Gamma-energy (keV)	μ/ρ (cm^2/g)	μ(cm^{-1})	Samples		Correction factors
			no.	thickness h (cm)	
139.68	0.3122	1.662	1	0.1863	1.163
			2	0.0948	1.081
264.6	0.1319	0.702	1	0.1863	1.067
			2	0.0948	1.034

fluence fluctuation factor:

$$K = \left[\sum_{i}^{L} \Phi_i (1 - e^{-\lambda \Delta t_i}) e^{-\lambda T_i}\right] \Big/ \Phi S,$$

where L is the number of time intervals into which the irradiation time is divided; Δt_i is the duration of the i-th time interval; T_i is the time interval from the end of the i-th interval to the end of irradiation; Φ_i is the neutron flux averaged over the sample during Δt_i; Φ is the neutron flux averaged over the sample during the total irradiation time T. F is the total correction factor of the activity:

$$F = f_s \times f_g, \tag{2}$$

where f_s and f_g are correction factors for the self-absorption of the sample at a given gamma-ray energy and the counting geometry, respectively. The gamma ray attenuation correction factor in the Ge pellet, f_s and the geometry correction, f_g were calculated by eqs. (3) and (4),

$$f_s = \frac{\mu h}{1 - \exp(-\mu h)}, \tag{3}$$

$$f_g = \frac{(D + h/2)^2}{D^2}, \tag{4}$$

where μ (in cm^{-1}) is the linear attenuation coefficient in Ge for gamma rays at each of the photon energies, E (see table 2), h (in cm) is the thickness of the sample and D (in cm) is the distance from the measured sample to the surface of the Ge crystal. The mass attenuation coefficients, μ/ρ for the germanium, which are 0.3122 and 0.1319 cm^2/g at gamma-ray energies of 139.68 and 264.6 keV respectively, were obtained by interpolating values from the literature [20]. The linear attenuation coefficients in Ge were then calculated according to $\rho = 5.323\,\mathrm{g/cm^3}$. The correction factors at 139.68 and 264.6 keV gamma-rays are given in table 2.

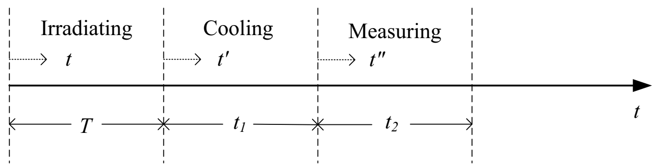

Fig. 4. Sketch map of the time during which the sample is irradiated, cooled, and measured.

While calculating the cross sections of the ^{76}Ge(n, 2n) ^{75g}Ge reaction, C_x in (1) should be the result of the measured full-energy peak area (at 264.6 keV γ-ray) minus the contribution from ^{75m}Ge via $^{75m}\mathrm{Ge} \xrightarrow{\mathrm{IT}(99.97\%)} {}^{75g}\mathrm{Ge}$ (counting C'_{mg}). According to the regulation of growth and decay of artificial radioactive nuclide we can deduce a formula to calculate the number of the daughter nucleus ^{75m}Ge at any moment t during the irradiation (see fig. 4) as follows:

$$N_m(t) = \frac{N\phi_0\sigma_m}{\lambda_m}(1 - e^{-\lambda_m t}), \tag{5}$$

where σ_m is the cross sections for formation of the metastable, λ_m is the decay constant of this state, ϕ_0 is the mean neutron flux in neutrons/cm^2/sec, and N is the number of target nuclei.

At any moment t during the irradiation, the number of ^{75g}Ge from the ^{75m}Ge $\rightarrow$ ^{75g}Ge procedure meets the following equation:

$$\frac{\mathrm{d}N_g(t)}{\mathrm{d}t} = P_{mg}\lambda_m N_m(t) - \lambda_g N_g(t), \tag{6}$$

where P_{mg} is the fraction of disintegrations of the metastable state that produces ground state nuclides (branching ratio), λ_g is the decay constant of ^{75g}Ge.

Using eqs. (5) and (6) and the initial condition: $t = 0$, $N_g(0) = 0$, and working out $N_g(t)$,

$$N_g(t) = N\phi_0\sigma_m P_{mg}\left[\left(\frac{1}{\lambda_g} - \frac{1}{\lambda_g - \lambda_m}e^{-\lambda_m t}\right) - \left(\frac{1}{\lambda_g} - \frac{1}{\lambda_g - \lambda_m}\right)e^{-\lambda_g t}\right]. \quad (7)$$

At the moment of the end of the irradiation ($t = T$), the numbers of $^{75\mathrm{m}}$Ge and $^{75\mathrm{g}}$Ge from $^{75\mathrm{m}}\mathrm{Ge} \to {}^{75\mathrm{g}}\mathrm{Ge}$ are $N_m(T)$ and $N_g(T)$, respectively, which can be obtained by using eqs. (5) and (7).

At any moment t' after the irradiation, the number of $^{75\mathrm{m}}$Ge is

$$N_m(t') = N_m(T)e^{-\lambda_m t'} = \frac{N\phi_0\sigma_m}{\lambda_m}(1 - e^{-\lambda_m T})e^{-\lambda_m t'}. \quad (8)$$

At any moment after the irradiation t', the number of $^{75\mathrm{g}}$Ge from $^{75\mathrm{m}}\mathrm{Ge} \to {}^{75\mathrm{g}}\mathrm{Ge}$ meets eq. (6). Using eqs. (6) and (8) and the initial condition $t' = 0$, $N_g(0) = N_g(T)$ (the number of $^{75\mathrm{g}}$Ge from $^{75\mathrm{m}}\mathrm{Ge} \to {}^{75\mathrm{g}}\mathrm{Ge}$ is equal at the end of the irradiation and the start of cooling) and working out $N_g(t')$,

$$N_g(t') = \frac{N\phi_0\sigma_m P_{mg}}{\lambda_g - \lambda_m}\left[(1 - e^{-\lambda_m T})e^{-\lambda_m t'} - \frac{\lambda_m}{\lambda_g}(1 - e^{-\lambda_g T})e^{-\lambda_g t'}\right]. \quad (9)$$

Let t' in eqs. (8) and (9) equal $t''+t_1$. t_1 is the time interval from the end of the irradiation to the start of counting. We can obtain the number of $^{75\mathrm{m}}$Ge at any moment t'' after beginning to detect the characteristic γ ray of $^{75\mathrm{m}}$Ge

$$N_m(t'') = \frac{N\phi_0\sigma_m}{\lambda_m}(1 - e^{-\lambda_m T})e^{-\lambda_m t_1}e^{-\lambda_m t''} \quad (10)$$

and the number of $^{75\mathrm{g}}$Ge from the $^{75\mathrm{m}}\mathrm{Ge} \to {}^{75\mathrm{g}}\mathrm{Ge}$ procedure at any moment t'' after beginning to detect the characteristic γ ray of $^{75\mathrm{g}}$Ge

$$N_g(t'') = \frac{N\phi_0\sigma_m P_{mg}}{\lambda_g - \lambda_m}\left[(1 - e^{-\lambda_m T})e^{-\lambda_m t_1}e^{-\lambda_m t''} - \frac{\lambda_m}{\lambda_g}(1 - e^{-\lambda_g T})e^{-\lambda_g t_1}e^{-\lambda_g t''}\right]. \quad (11)$$

During the period t_2 of detecting the characteristic γ ray, the full-energy peak (FEP) counts C'_m of the characteristic γ ray of $^{75\mathrm{m}}$Ge and C'_{mg} of the characteristic γ ray of $^{75\mathrm{g}}$Ge from the $^{75\mathrm{m}}\mathrm{Ge} \to {}^{75\mathrm{g}}\mathrm{Ge}$ procedure are

$$C'_m = \int_0^{t_2} \lambda_m I_m \varepsilon_m N_m(t'')\mathrm{d}t'' = \frac{I_m\varepsilon_m N\phi_0\sigma_m}{\lambda_m}\left[(1 - e^{-\lambda_m T})e^{-\lambda_m t_1}(1 - e^{-\lambda_m t_2})\right], \quad (12)$$

$$C'_{mg} = \int_0^{t_2} \lambda_g I_g \varepsilon_g N_g(t'')\mathrm{d}t'' = \frac{I_g\varepsilon_g N\phi_0\sigma_m P_{mg}}{\lambda_g - \lambda_m}\left[\frac{\lambda_g}{\lambda_m}(1 - e^{-\lambda_m T})e^{-\lambda_m t_1}(1 - e^{-\lambda_m t_2}) - \frac{\lambda_m}{\lambda_g}(1 - e^{-\lambda_g T})e^{-\lambda_g t_1}(1 - e^{-\lambda_g t_2})\right]. \quad (13)$$

Using eqs. (12) and (13), C'_{mg} can be written as

$$C'_{mg} = \frac{P_{mg}\varepsilon_g I_g C'_m(\lambda_g^2 S_m D_m - \lambda_m^2 S_g D_g)}{(\lambda_g - \lambda_m)S_m D_m I_m \varepsilon_m \lambda_g K_m}, \quad (14)$$

where $S_m = 1-e^{-\lambda_m T}$ and $S_g = 1-e^{-\lambda_g T}$; I_m and I_g are the gamma ray intensities of the measured metastable and ground state, respectively; ε_m and ε_g are the full-energy peak efficiencies of the characteristic gamma-rays of the measured metastable and ground state, respectively; K_m is neutron fluence fluctuation factor of the metastable state; D_m and D_g can be written as

$$D_m = e^{-\lambda_m t_1} - e^{-\lambda_m(t_1+t_2)}, \qquad D_g = e^{-\lambda_g t_1} - e^{-\lambda_g(t_1+t_2)}$$

3 Nuclear model calculations

The excitation functions for the reactions were studied theoretically using the numerical nuclear model code TALYS-1.8 [21]. The theoretical calculations were computed using the default parameter values and only changing the choice of the level density models. The level density parameters were calculated using the six different choices of level density models available in TALYS-1.8. The six level density models are given in table 3.

4 Discussions

The cross sections measured in this work are presented in table 4. The uncertainty analysis was carried out using the quadrature method [22]. The principal sources of uncertainty and their estimated values are given in table 5. The total uncertainty lies between 4.5 and 8.7%. The small contribution to the gamma ray activity of products from the $^{74}\mathrm{Ge}(\mathrm{n},\gamma)$ reaction could be ignored because of the very small cross section of the (n,γ) reaction in the region of 14 MeV. Furthermore, samples were wrapped in a cadmium foil in order to reduce the contribution of thermal and epithermal effects. For the $^{76}\mathrm{Ge}(\mathrm{n},2\mathrm{n})^{75\mathrm{m,g}}\mathrm{Ge}$ reactions the cross sections slightly increase with the increasing neutron energy. The various reactions are discussed below.

Table 3. The six different level density models.

Level density model	Describes
ldmodel 1	the constant temperature and Fermi gas model, where the constant temperature model is used in the low excitation region and the Fermi-gas model in the high excitation energy region. The transition energy is around the neutron separation energy.
ldmodel 2	the back-shifted Fermi gas model.
ldmodel 3	the generalized superfluid model.
ldmodel 4	composed of microscopic level densities (Skyrme force) from Goriely's tables [23].
ldmodel 5	composed of microscopic level densities (Skyrme force) from Hilaire's combinatorial tables [23].
ldmodel 6	microscopic level densities (temperature dependent HFB, Gogny force) from Hilaire's combinatorial tables [23].

Table 4. Summary of cross section measurements.

Reaction	Cross sections (in mb) at various neutron energies (in MeV)		
	13.5 ± 0.2	14.1 ± 0.2	14.8 ± 0.2
$^{76}\mathrm{Ge(n,2n)}^{75\mathrm{m}}\mathrm{Ge}$	870 ± 39	899 ± 41	910 ± 44
$^{76}\mathrm{Ge(n,2n)}^{75\mathrm{g}}\mathrm{Ge}$	376 ± 31	380 ± 33	381 ± 30
$^{76}\mathrm{Ge(n,2n)}^{75}\mathrm{Ge}$	1246 ± 70	1279 ± 74	1291 ± 74
$^{93}\mathrm{Nb(n,2n)}^{92\mathrm{m}}\mathrm{Nb}$	457.9 ± 6.8 [19]	459.8 ± 6.8 [19]	459.7 ± 5.0 [19]

Table 5. Principal sources of uncertainty and their estimated values in cross section measurements.

Source of uncertainty	Uncertainty %
counting statistics	0.5–3.2
standard cross sections	1.1–1.5
isotopic abundance	1.6
detector efficiency	2.0–3.0
weight of samples	0.1
self-absorption of gamma-ray	~ 0.5
relative gamma-ray intensity	~ 1.0
half-life	0.05–1.1
uncertainties of irradiation, cooling and measuring times	0.1–0.5
total uncertainty	4.5–8.7

4.1 $^{76}\mathrm{Ge(n,2n)}^{75\mathrm{m}}\mathrm{Ge}$ reaction

In the present work, an intensity of $I_\gamma = 39.51\%$ of the 139.68 keV gamma-ray emitted in the decay of $^{75\mathrm{m}}$Ge was used to deduce the value of the $^{76}\mathrm{Ge(n,2n)}^{75\mathrm{m}}\mathrm{Ge}$ reaction cross section. Vanska and Rieppo [9] and Hlavac *et al.* [12] used $I_\gamma = 34\%$, Kasugai *et al.* [10] used $I_\gamma = 38.8\%$ for the same ray (139.68 keV) (see table 6). Thus, these data are normalized with respect to the latest γ-ray branching of 39.51% [18]. For this reaction, it's threshold energy is 9.694 MeV. In order to avoid the effect of low-energy neutrons, the near threshold $^{93}\mathrm{Nb(n,2n)}^{92\mathrm{m}}\mathrm{Nb}$ (E_{th} = 8.972 MeV) monitor reaction was selected. Whereas, Vanska and Rieppo [9], Kasugai *et al.* [10], Mangal and Gill [11], Hlavac *et al.* [12], and Attar *et al.* [14] used the lower threshold $^{27}\mathrm{Al(n,p)}^{27}\mathrm{Mg}$ (E_{th} = 1.896 MeV) and Dzysiuk *et al.* [13] used $^{27}\mathrm{Al(n,}\alpha)^{24}\mathrm{Na}$ (E_{th} = 3.249 MeV) monitor reactions (see table 6). Our results are plotted in fig. 5 along with all the other data [7–14]. In the energy region between 13 and 14 MeV our values are in agreement with those of Bormann *et al.* [8] within their experimental uncertainties. At 14.8 MeV, present data is in agreement with the results of Kasugai *et al.* [10], Hlavac *et al.* [12] and Attar *et al.* [14] within the experimental uncertainties. The shapes of the excitation curves of the TALYS-1.8 calculation also exhibit a trend similar to Bormann *et al.* [8], Kasugai *et al.* [10], Attar *et al.* [14], and the present data set. Between 13 and 15 MeV the TALYS-1.8 calculations with ldmodels 1, 5, and 6 agree very well with our measured data within the reported data uncertainties.

4.2 $^{76}\mathrm{Ge(n,2n)}^{75\mathrm{g}}\mathrm{Ge}$ reaction

Concerning the $^{76}\mathrm{Ge(n,2n)}^{75\mathrm{g}}\mathrm{Ge}$ reaction, there are three earlier measurements that can be found in the litera-

Table 6. Summary of ^{76}Ge(n, 2n) reaction cross sections from previous measurements.

Reaction	Method	Decay data	Detector	Monitor reaction	Reference
^{76}Ge(n, 2n)^{75m}Ge	activation	no information	GeLi	^{63}Cu(n, 2n)^{62}Cu	ref. [7]
	activation	$T_{1/2} = 48.2$ s	NaI	No information	ref. [8]
	activation	$T_{1/2} = 49$ s, $E_\gamma = 136$ keV, $I_\gamma = 34\%$	GeLi	^{27}Al(n, p)^{27}Mg	ref. [9]
	activation	$T_{1/2} = 47.7$ s, $E_\gamma = 139.5$ keV, $I_\gamma = 38.8\%$	HPGe	^{27}Al(n, p)^{27}Mg	ref. [10]
	activation	$T_{1/2} = 48$ s	NaI	^{27}Al(n, p)^{27}Mg	ref. [11]
	activation	$T_{1/2} = 48$ s, $E_\gamma = 139$ keV, $I_\gamma = 34\%$	GeLi	^{27}Al(n, p)^{27}Mg	ref. [12]
	activation	$T_{1/2} = 47.7$ s	HPGe	^{27}Al(n, α)^{24}Na	ref. [13]
	activation	$T_{1/2} = 47.7$ s, $E_\gamma = 139.7$ keV, $I_\gamma = 39.4\%$	HPGe	^{27}Al(n, p)^{27}Mg	ref. [14]
^{76}Ge(n, 2n)^{75g}Ge	activation	no information	GeLi	^{63}Cu(n, 2n)^{62}Cu	ref. [7]
	activation	$T_{1/2} = 82.8$ min, $E_\gamma = 264.8$ keV ($I_\gamma = 11.0\%$), $E_\gamma = 199.2$ keV ($I_\gamma = 1.4\%$)	GeLi	^{27}Al(n, p)^{27}Mg	ref. [9]
	activation	$T_{1/2} = 82.78$ min, $E_\gamma = 264.0$ keV, $I_\gamma = 11.4\%$	HPGe	^{27}Al(n, p)^{27}Mg	ref. [14]
^{76}Ge(n, 2n)^{75}Ge	activation	$T_{1/2} = 82$ min	Boron counter	No information	ref. [24]
	activation	$T_{1/2} = 82.2$ min, $E_\gamma = 265$ keV, $I_\gamma = 11.0\%$	GeLi	^{70}Ge(n,2n)^{69}Ge	ref. [25]
	activation	no information	NaI	counting the associated alpha particles	ref. [26]
	activation	no information	Ge	^{56}Fe(n, p)^{56}Mn	ref. [27]
	activation	$T_{1/2} = 1.38$ h, $E_\gamma = 264.7$ keV, $I_\gamma = 11.3\%$	GeLi	^{27}Al(n, α)^{24}Na	ref. [28]
	activation	$T_{1/2} = 81.79$ min	NaI	^{63}Cu(n, 2n)^{62}Cu	ref. [29]
	activation	$T_{1/2} = 78$ min	GEMUC	^{56}Fe(n, p)^{56}Mn	ref. [30]
	activation	no information	HPGe	^{27}Al(n, α)^{24}Na	ref. [31]
	activation	$T_{1/2} = 82.78$ min, $E_\gamma = 264.6$ keV, $I_\gamma = 11.4\%$	HPGe	^{93}Nb(n, 2n)^{92m}Nb	ref. [32]
	activation	$T_{1/2} = 82.78$ min, $E_\gamma = 264.6$ keV, $I_\gamma = 11.4\%$	HPGe	^{27}Al(n, α)^{24}Na	ref. [33]

ture [7,9,14]. In the present work, the 264.6 keV ($I_\gamma = 11.4\%$) gamma-ray emitted in the ^{75g}Ge decay was used to deduce the value of the ^{76}Ge(n, 2n)^{75g}Ge reaction cross section. The contribution of the ^{76}Ge(n, 2n)^{75m}Ge reaction via IT (isomeric transition, 99.97%) was subtracted using eq. (14). Figure 6 shows the excitation function of the ^{76}Ge(n, 2n)^{75g}Ge reaction. Between 13 and 15 MeV, the measured data for the ^{76}Ge(n, 2n)^{75g}Ge reaction cross sections can be grouped into two bands which differ by about 80%. The large discrepancies are probably due to the different deducting methods of excited states. Between 13 and 15 MeV, the Talys-1.8 calculations with ldmodels 1–6 are lower than all the results of papers in the literature [7,9,14], but the TALYS-1.8 calculations with ldmodel 1 (the constant temperature and Fermi gas model) agree very well with our data, whilst the results by Casanova and Sanchez [7], Vanska and Rieppo [9], and Attar *et al.* [14] are about 60–90% higher than our data and TALYS-1.8 calculations. For this reaction, other previous authors [8,10–13] only reported cross section values of the excited state and did not give cross section values of the ground state.

4.3 ^{76}Ge(n, 2n)^{75}Ge reaction

The present cross section data for the ^{76}Ge(n, 2n)^{75}Ge reaction are shown in fig. 7 together with the results of the TALYS-1.8 calculation with ldmodels 1, 2, 3, 4, 5, and 6 (given as continuous lines) and earlier measurements [9, 12,13,24–33]. It can be seen that in the 13 to 15 MeV energy range our data are consistent with the results of TALYS-1.8 calculations using ldmodels 1, 2, 4, 5, and 6 within the experimental uncertainties.

4.4 Isomeric cross section ratio

The isomeric cross section ratio σ_m/σ_g for the isomeric pair ^{75m,g}Ge produced in the (n,2n) reaction on ^{76}Ge was

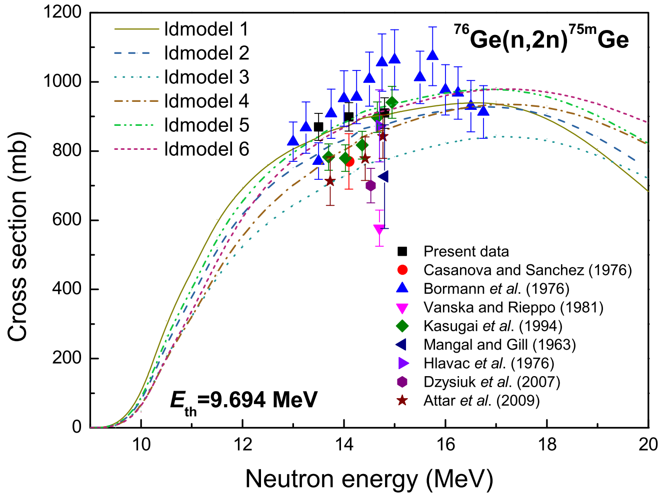

Fig. 5. Excitation function of the ^{76}Ge(n, 2n)^{75m}Ge reaction compared with the present measured data and the literature normalized data.

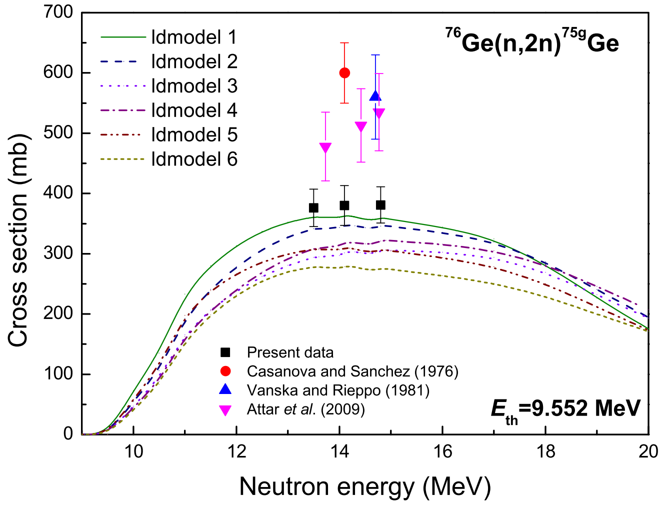

Fig. 6. Excitation function of the ^{76}Ge(n, 2n)^{75g}Ge reaction with the present measured data and the literature data.

measured. The obtained cross section ratios are 2.3 ± 0.2, 2.4 ± 0.2 and 2.4 ± 0.2 at neutron energies of 13.5 ± 0.2, 14.1 ± 0.2, and 14.8 ± 0.2 MeV, respectively. The experimental data and the TALYS-1.8 calculations are shown together in fig. 8. It can be seen that our results agree well with the result of Bhattacharyya *et al.* [34], and the data from the TALYS-1.8 calculations with ldmodel 1, 2 and 3.

The isomeric cross section ratio determined in this work has a slightly increasing trend with the increasing neutron energy, suggesting that at higher excitation energies the formation of the high-spin isomer ($7/2 \rightarrow 1/2$) is more favored. This trend is similar to that for several other neutron- and charged-particle–induced reactions near thresholds [35–44]. In the range of 13–15 MeV, the calculated isomeric cross section ratio shows the same slightly increasing trend for the six ldmodels. Our data and the results of TALYS-1.8 with ldmodels 1, 2, and 3 are somewhat lower than the data of Hlavac *et al.* [12], Okumura [26], Birn *et al.* [28], while they are higher than the results of Vanska and Rieppo [9] and Mangal and Gill [11].

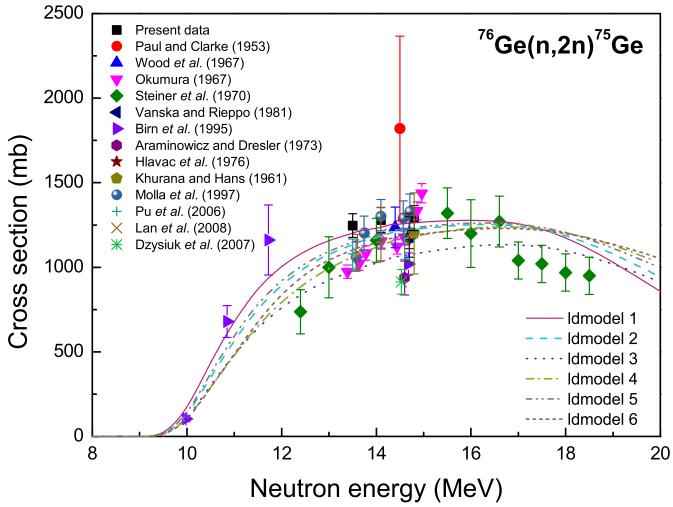

Fig. 7. Excitation function of the ^{76}Ge(n, 2n)^{75}Ge reaction.

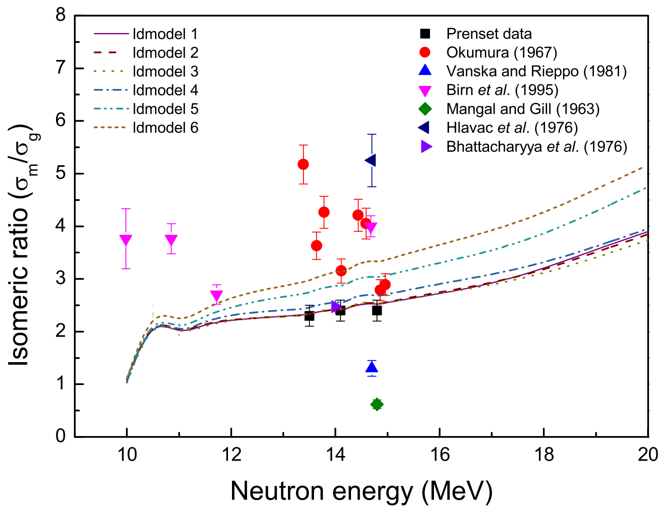

Fig. 8. Cross section ratio of the ^{76}Ge(n, 2n)^{75m}Ge and ^{76}Ge(n, 2n)^{75g}Ge reactions plotted as a function of the neutron energy.

5 Conclusions

In the present paper, a methodical experimental campaign and TALYS-1.8 code calculations with different level density models have been carried out. Activation cross sections for ^{76}Ge(n, 2n)^{75m}Ge, ^{76}Ge(n, 2n)^{75g}Ge, and ^{76}Ge(n, 2n)^{75}Ge reactions as well as isomeric cross section ratios for ^{76}Ge(n, 2n)^{75m,g}Ge reactions induced by 13.5, 14.1 MeV, and 14.8 MeV neutrons have been measured using the latest decay data, and by taking into account the contribution of the metastable state in the case of unstable ground state formation cross section. In order to avoid the effect of low energy neutrons, the near threshold ^{93}Nb(n, 2n)^{92m}Nb ($E_{th} = 8.972$ MeV) monitor reaction was selected, samples were wrapped in a cadmium foil and the new T-Mo target was used. The constant temperature and Fermi gas model (ldmodel 1) is to be preferred for $^{76}\mathrm{Ge(n, 2n)}^{75\mathrm{m,g}}\mathrm{Ge}$ reactions. The results were compared with previous experimental results reported in the literature and theoretical nuclear model calculations computed using TALYS-1.8. A detailed comparison with previously reported cross sections reveals that the discrepancies in the historic data could be due to: 1) the decay data (half-life and ray intensity) used in the determination of the cross sections; 2) the system difference caused by different measuring methods (radiation detector and neutron monitoring method) and experimental conditions (neutron field characteristics); and 3) interfering reactions. The experimental results presented here may be used to more accurately describe the reaction processes and verify statistical model parameters used in their theoretical representation.

We would like to thank the Intense Neutron Generator group at Chinese Academy of Engineering Physics for performing the irradiations. This work was supported by the National Natural Science Foundation of China (Grant No. 11565012).

References

1. M. Bostan, S.M. Qaim, Phys. Rev. C **49**, 266 (1994).
2. CINDA-A: The index to literature and computer files on microscopic neutron data, (International Atomic Energy Agency, Vienna, 2000).
3. V. Mclane, C.L. Dunford, P.F. Rose, *Neutron cross sections*, Vol. **2** (Academic, New York, 1988).
4. K. Heyde, J.L. Wood, Rev. Mod. Phys. **83**, 1467 (2011).
5. Toh *et al.*, Phys. Rev. C **87**, 041304(R) (2013).
6. A.S. Davydov, G.F. Filipov, Nucl. Phys. **8**, 237 (1958).
7. J.L. Casanova, M.L. Sanchez, An. Fis. Quim. **3**, 186 (1976).
8. M. Bormann *et al.*, Progress report, Report from Euratom-countries + Euratom to EANDC, No. 76 (1967) p. 51.
9. R. Vanska, R. Rieppo, Nucl. Instrum. Methods **179**, 525 (1981).
10. Y. Kasugai *et al.*, Am. Rev. Respir. Dis. **132**, 248 (1994).
11. S.K. Mangal, P.S. Gill, Nucl. Phys. **49**, 510 (1963).
12. S. Hlavac *et al.*, Acta Phys. Slov. **26**, 64 (1976).
13. N.R. Dzysiuk *et al.*, Yad. Fiz. Energ. **8**, 68 (2007).
14. F.M.D. Attar *et al.*, Nucl. Phys. A **828**, 253 (2009).
15. F. Zhou *et al.*, Phys. Rev. C **80**, 054615 (2009).
16. J. Luo *et al.*, Appl. Radiat. Isot. **66**, 1920 (2008).
17. J. Luo *et al.*, Radiochim. Acta **101**, 607 (2013).
18. Evaluated Nuclear Structure Data File (ENSDF), `http://www.nndc.bnl.gov/ensdf/`.
19. M. Wagner *et al.*, *Physik Daten-Physics Data, Evaluation of Cross Sections for 14 important Neutron Dosimetry Reactions*, Fachinformationszentrum Karlsruhe, Gesellschaft für wissenschaftlich-technische Information mbH, Federal Republic of Germany. No.13-5 (1990).
20. J.H. Hubbell, S.M. Seltzer, *Tables of x-ray mass attenuation coefficients and mass energy-absorption coefficients from* 1 keV *to* 20 MeV *for elements* $Z = 1$ *to* 92 *and* 48 *additional substances of dosimetric interest* (1996) `http://physics.nist.gov/PhysRefData/XrayMassCoef/tab3.html`.
21. A. Koning, S. Hilaire, S. Goriely, *TALYS-1.8, A Nuclear Reaction Program*, NRG-1755 ZG Petten, The Netherlands (2015) `http://www.talys.eu`.
22. J.R. Taylor, *An Introduction to Uncertainty Analysis* (University Science Books, Mill Valley, California, 1982).
23. RIPL-2 Reference Input Parameter Library, IAEA, A-1400 Vienna, IAEA-NDS, `http://www-nds.iaea.org/RIPL-2/`.
24. E.B. Paul, R.L. Clarke, Can. J. Phys. **31**, 267 (1953).
25. R.E. Wood *et al.*, Phys. Rev. **154**, 1108 (1967).
26. S. Okumura, Nucl. Phys. A **93**, 74 (1967).
27. E. Steiner *et al.*, Helv. Phys. Acta **43**, 17 (1970).
28. I.G. Birn *et al.*, Phys. Rev. C **52**, 2546 (1995).
29. J. Araminowicz, J. Dresler, *Investigation of the (n,2n) reaction with 14.6 MeV neutrons*, Progress Report, Inst. Badan Jadr. (Nucl. Res.), Swierk+Warsaw, Repts., No. 1464 (1973) p.14.
30. C.S. Khurana, H.S. Hans, Nucl. Phys. **28**, 560 (1961).
31. N.I. Molla *et al.*, in *Conference on Nuclear Data for Science and Technology, Trieste 1997*, Vol. **1** (SIF, 1997) p.517.
32. Z. Pu *et al.*, High. Energy Phys. Nucl. Phys. **30**, 1171 (2006) in Chinese.
33. C. Lan *et al.*, Ann. Nucl. Energy **35**, 2105 (2008).
34. P. Bhattacharyya *et al.*, *Decay of the 83 min Ge-75 and energy levels and gamma-transitions in As-75*, in *Nuclear Physics and Solid State Physics Symposium, Ahmedabad*, Vol. **2**, Part 19B (Department of Atomic Energy, Bombay, India, 1976) p. 316.
35. S.M. Qaim, A. Mushtaq, M. Uhl, Phys. Rev. C **38**, 645 (1988).
36. N.I. Molla, S.M. Qaim, M. Uhl, Phys. Rev. C **42**, 1540 (1990).
37. S.M. Qaim *et al.*, Phys. Rev. C **42**, 363 (1990).
38. S. Sudár, F. Szelecsényi, S.M. Qaim, Phys. Rev. C **48**, 3115 (1993).
39. F. Cserpák *et al.*, Phys. Rev. C **49**, 1525 (1994).
40. I.G. Birn *et al.*, Phys. Rev. C **52**, 2546 (1995).
41. S. Sudár, S.M. Qaim, Phys. Rev. C **53**, 2885 (1996).
42. C.D. Nesaraja, S. Sudár, S.M. Qaim, Phys. Rev. C **68**, 024603 (2003).
43. S. Sudár, S.M. Qaim, Phys. Rev. C **73**, 034613 (2006).
44. M. Al-Abyad *et al.*, Phys. Rev. C **73**, 064608 (2006).